AMERICAN SOCIETY FOR MICROBIOLOGY | Applied and Environmental Microbiology®

PHYSIOLOGY

# Isolation, Genomic Sequence and Physiological Characterization of *Parageobacillus* sp. G301, an Isolate Capable of Both Hydrogenogenic and Aerobic Carbon Monoxide Oxidation

**Yoshinari Imaura,[a] Shunsuke Okamoto,[a] Taiki Hino,[a] Yusuke Ogami,[a] Yuka Adachi Katayama,[a] Ayumi Tanimura,[a] Masao Inoue,[a,b,c] Ryoma Kamikawa,[a] Takashi Yoshida,[a] Yoshihiko Sako[a]**

[a]Graduate School of Agriculture, Kyoto University, Kyoto, Japan
[b]R-GIRO, Ritsumeikan University, Kusatsu, Shiga, Japan
[c]College of Life Sciences, Ritsumeikan University, Kusatsu, Shiga, Japan

**ABSTRACT** Prokaryotes that can oxidize carbon monoxide (CO oxidizers) can use this gas as a source of carbon or energy. They oxidize carbon monoxide with carbon monoxide dehydrogenases (CODHs): these are divided into nickel-containing CODH (Ni-CODH), which are sensitive to $O_2$, and molybdenum-containing CODH (Mo-CODH), which can function aerobically. The oxygen conditions required for CO oxidizers to oxidize CO may be limited, as those which have been isolated and characterized so far contain either Ni- or Mo-CODH. Here, we report a novel CO oxidizer, *Parageobacillus* sp. G301, which is capable of CO oxidation using both types of CODH based on genomic and physiological characterization. This thermophilic, facultatively anaerobic *Bacillota* bacterium was isolated from the sediments of a freshwater lake. Genomic analyses revealed that strain G301 possessed both Ni-CODH and Mo-CODH. Genome-based reconstruction of its respiratory machinery and physiological investigations indicated that CO oxidation by Ni-CODH was coupled with $H_2$ production (proton reduction), whereas CO oxidation by Mo-CODH was coupled with $O_2$ reduction under aerobic conditions and nitrate reduction under anaerobic conditions. G301 would thus be able to thrive via CO oxidation under a wide range of conditions, from aerobic environments to anaerobic environments, even with no terminal electron acceptors other than protons. Comparative genome analyses revealed no significant differences in genome structures and encoded cellular functions, except for CO oxidation between CO oxidizers and non-CO oxidizers in the genus *Parageobacillus*; CO oxidation genes are retained exclusively for CO metabolism and related respiration.

**IMPORTANCE** Microbial CO oxidation has received much attention because it contributes to global carbon cycling in addition to functioning as a remover of CO, which is toxic to many organisms. Some microbial CO oxidizers, including both bacteria and archaea, exhibit sister relationships with non-CO oxidizers even in genus-level monophyletic groups. In this study, we demonstrated that a new isolate, *Parageobacillus* sp. G301, is capable of both anaerobic (hydrogenogenic) and aerobic CO oxidation, which has not been previously reported. The discovery of this new isolate, which is versatile in CO metabolism, will accelerate research on CO oxidizers with diverse CO metabolisms, expanding our understanding of microbial diversity. Through comparative genomic analyses, we propose that CO oxidation genes are not essential genetic elements in the genus *Parageobacillus*, providing insights into the factors which shape the punctate distribution of CO oxidizers in the prokaryote tree, even in genus-level monophyletic groups.

**KEYWORDS** carbon monoxide dehydrogenase, carbon monoxide metabolism, *Parageobacillus*

**Editor** Ning-Yi Zhou, Shanghai Jiao Tong University



Address correspondence to Takashi Yoshida, yoshida.takashi.7a@kyoto-u.ac.jp.

The authors declare no conflict of interest.

**Received** 16 February 2023
**Accepted** 6 May 2023
**Published** 23 May 2023

Although carbon monoxide is toxic to many organisms (1, 2), some prokaryotes called CO oxidizers perform CO oxidation for energy conservation (3–6). Indeed, because CO is a favorable electron donor (reduction potential [$E^{o\prime}$] of −520 mV for the $CO/CO_2$ redox pair) (7, 8), CO oxidation can be coupled with the reduction of various terminal electron acceptors in CO oxidizers (3, 9–12). In addition to contributing to the carbon cycle by consuming atmospheric CO (3), CO oxidizers may benefit surrounding organisms by removing toxic amounts of CO (13). There are two types of carbon monoxide dehydrogenase (CODH), the key enzyme in CO oxidation: nickel-containing CODH (Ni-CODH) (14) and molybdenum-containing CODH (Mo-CODH) (15).

The catalytic subunit of Ni-CODH is divided into two types: CooS, which is frequently found in bacteria, and Cdh, almost all of which are found in archaea (16). Ni-CODHs are categorized into eight clades based on their phylogenetic relationships and active site motifs: clade A corresponds to Cdh, and clades B to H correspond to CooS (14, 16, 17). CO oxidizers containing *cooS/cdh* couple CO oxidation with the reduction of one or more terminal electron acceptors, including protons, $CO_2$, fumarate, sulfate, nitrate, and Fe(III) (4, 7, 18). One of the most well-known of these is the hydrogenogenic CO oxidizer, which couples CO oxidation with proton reduction to generate hydrogen ($H_2$). Physiological characterization was performed on 32 isolates of hydrogenogenic CO oxidizers from five phyla: *Bacillota*, *Pseudomonadota*, *Dictioglomi*, *Euryarchaeota*, and *Crenarchaeota* (7). Most hydrogenogenic CO oxidizers possess *cooS/cdh* in a gene cluster composed of *cooS/cdh*; *cooC*, which encodes a maturation factor of CooS (19); *cooF*, which encodes a ferredoxin-like protein (20); and genes encoding energy-converting hydrogenases (ECH) (*coo–ech* gene cluster). ECH performs proton reduction associated with ion translocation and contributes to energy conservation (21, 22).

Mo-CODHs can be divided into two groups: form I and form II Cox. This classification is based on the phylogeny and active site motifs (AYXCSFR for form I, AYRGAGR for form II) of the large subunit CoxL (3, 23). The gene of form I CoxL is regarded as a marker of CO oxidation; however, it is uncertain whether all form II Cox-bearing prokaryotes can oxidize CO (24). CO oxidation by form I Cox can be coupled with one or more terminal electron acceptors, including $O_2$, nitrate, and perchlorate (9, 10, 25). During electron transport, the quinone cycle generates a proton motive force that contributes to energy conservation (26). Heterotrophic CO oxidizers with form I Cox utilize CO as an energy source to survive under energy-limited conditions (25), whereas autotrophic CO oxidizers use CO as a source of both energy and carbon (27, 28).

*cooS/cdh* is found in the genomes of facultative and obligate anaerobes (7), possibly reflecting the sensitivity of Ni-CODHs to $O_2$ (29). Form I *coxL* is found in the genomes of (micro)aerobes (3, 30). To the best of our knowledge, no single prokaryote that can perform both Ni-CODH- and Mo-CODH-mediated CO oxidation has yet been reported. *cooS/cdh* and form I *coxL* demonstrate many examples of sister relationships of CO oxidizers and non-CO oxidizers in the phylogenetic trees of various genera, such as *Moorella* (with *cooS/cdh*) and *Aminobacter* (with form I *cox*) (31, 32). The key factors shaping punctate distributions in the tree of prokaryotes remain unclear, but could be revealed by an investigation of a monophyletic group in which some species possess *cooS/cdh*, others possess form I *cox*, and the rest possess neither gene.

*Parageobacillus* of the phylum *Bacillota* is a bacterial genus comprising obligately aerobic or facultatively anaerobic thermophiles (33) and was recently reclassified from the genus *Geobacillus* (34, 35). It includes six species (*P. toebii*, *P. thermoglucosidasius*, *P. thermantarcticus*, *P. caldoxylosilyticus*, *P. galactosidasius*, and *P. yumthangensis*) and one genomospecies, *Parageobacillus genomospecies* 1 NUB3621 (36). Among these, *P. toebii*, *P. galactosidasius*, and *P. yumthangensis* have been proposed to be the same species (37). In addition, *Saccharococcus thermophilus*, another thermophilic *Bacillota* bacterium, has been proposed for re-classification as *Parageobacillus* (37).

Four *P. thermoglucosidasius* strains (strains DSM 2542$^T$, DSM 2543, DSM 6285, and TG4) have a *coo–ech* gene cluster and perform hydrogenogenic CO oxidation (38–40). According to our previous analysis, the *coo–ech* gene cluster encodes functional Coo/

ECH, and both *coo* and *ech* are required for hydrogenogenic CO oxidation (41). Conversely, the type strain of *P. toebii* was demonstrated to contain *coxMSL*, although their CO oxidation was not confirmed (38).

In this study, we report a new isolate, *Parageobacillus* sp. G301, closely related to *P. toebii*, that performs both hydrogenogenic and aerobic CO oxidation reactions. We expanded our knowledge of the physiological diversity, functional versatility, and evolution of CO oxidizers using comparative genomics. Additionally, we discuss the factors that contribute to the punctate distribution of *codh* genes in the tree of prokaryotes.

## RESULTS

**Isolation of strain G301.** CO oxidizers were enriched in the sediment of Unagi-ike (31°13′37″ N and 130°36′38″ E), a freshwater lake in Japan into which water flows from a hot spring, by cultivation at 65°C under atmospheric conditions with a $N_2$:CO ratio of 80:20. Following CO depletion and $H_2$ evolution, the liquid phase of the culture was streaked on an NBRC 802 agar plate (42) and incubated aerobically at 65°C. The strain G301 was isolated from a single colony. G301 cells were rod-shaped and measured 0.5 to 1.0 $\mu$m $\times$ 2.0 to 3.5 $\mu$m in size (Fig. S1). Further cultivation revealed that strain G301 was a facultatively anaerobic, hydrogenogenic CO oxidizer.

**General features of the G301 genome and phylogenetic relationships with other *Parageobacillus*.** The G301 genome comprised nine scaffolds with a total length of 3,483,861 bp and a G+C content of 41.79%. It contained 13 rRNA genes, 58 tRNA genes, 2,128 protein-coding genes with known functions, and 1,659 functionally unassigned open reading frames (ORFs) according to gene prediction using PATRIC (43).

In the 16S rRNA gene tree, strain G301 was distantly related to *P. thermoglucosidasius*, a well-characterized hydrogenogenic CO oxidizer (Fig. 1A). However, the closest relative of G301 remained unclear in this analysis. Thus, we performed a phylogenomic analysis using a concatenated data set of amino acid sequences of 1,505 single-copy core genes from 27 *Parageobacillus* strains. Of these strains, 1 and 7 were classified as *S. thermophilus* and "unclassified *Geobacillus*" in NCBI taxonomy (44), respectively. G301 was sister to the clade of *P. toebii*, *P. galactosidasius*, *P. yumthangensis*, *Geobacillus* sp. 44C, *Geobacillus* sp. NFOSA3, *Geobacillus* sp. E263, *Geobacillus* sp. WCH70, and *Geobacillus* sp. LYN3 with 100% bootstrap support (Fig. 1B). The average nucleotide identity (ANI) values between the G301 genome and those of *P. toebii*, *P. galactosidasius*, *P. yumthangensis*, and the 5 unclassified *Geobacillus* strains ranged from 96.0% to 97.1% (Table S1), which exceeded the 95% threshold for the same species (45).

**Genes involved in CO oxidation in G301.** To characterize the genes whose products contribute to CO oxidation, we searched *cooS* and form I *coxL* in the G301 genome. According to annotation using DFAST (46), *cooS* was present in BSDB01000001 (locus tag: PG301_04030, 373,389 to 375,311 bp) between *cooC* (PG301_04020) (19) and *cooF* (PG301_04040) (20) (Fig. 2A). Furthermore, 12 genes encoding hydrogenase (locus tag: PG301_04050–PG301_04160) were located downstream of *cooF* (Fig. 2A). The large subunit of hydrogenase encoded by PG301_04100 was classified as a [NiFe] Group 4a hydrogenase by HydDB (47). The composition of the genes corresponded to that of the *coo–ech* gene clusters (14, 16).

One form I *coxL* was also found in BSDB01000001 (locus tag: PG301_05530, 523,179 to 525,530 bp) (Fig. 2A). *coxM* (locus tag: PG301_05550) and *coxS* (locus tag: PG301_05540) genes, which encode the medium and small subunits of Cox, respectively (15), were located upstream of *coxL*. The genes downstream of *coxL* encoded CoxF, CoxG, CoxD, CoxE, *cytochrome c* oxidase assembly protein CtaG, CoxF, nucleotidyltransferase family protein MocA, molybdopterin adenylyltransferase MogA, and molybdopterin molybdenum transferase MoeA (locus tags: PG301_05520–PG301_05440). These genes encode accessory proteins of Cox or proteins associated with biosynthesis of the molybdenum cofactors, which may help in the maturation of Cox catalytic subunits. The gene organization of *cox*, including *coxM*, *coxS*, *coxL*, *coxD*, *coxE*, and *coxF*, was a common feature of the form I *cox* gene cluster (3). Additionally, another gene cluster comprising genes encoding cytochrome ubiquinol oxidase subunits CydA and CydB (locus tags: PG301_05590 and PG301_05580)

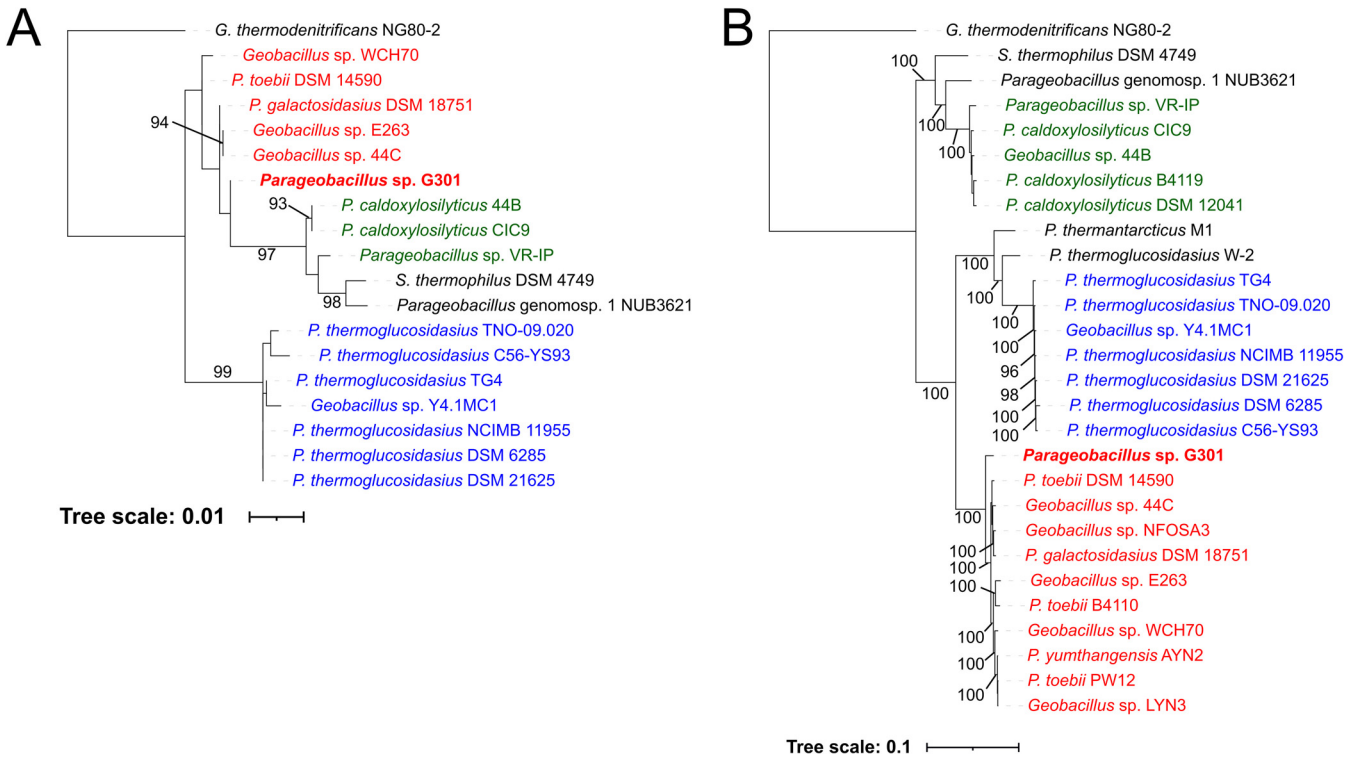


**FIG 1** (A) Maximum-likelihood trees of 18 *Parageobacillus* strains and *Geobacillus thermodenitrificans* inferred by 16S rRNA gene sequences. (B) Maximum-likelihood trees of 27 *Parageobacillus* strains and *G. thermodenitrificans* inferred by the amino acid sequences of 1,505 single-copy core genes. Bootstrap values over 90% are shown. Branch lengths represent the number of substitutions per site. Strains whose average nucleotide identity (ANI) values with G301 were higher than 95% are highlighted in red. Strains whose ANI values with *P. caldoxylosilyticus* DSM 12041 were higher than 95% are highlighted in green. Strains whose ANI values with *P. thermoglucosidasius* NCIMB 11955 were higher than 95% are highlighted in blue.

and their maturation factors CydC and CydD (locus tags: PG301_05570 and PG301_05560) was present upstream of *coxM* (Fig. 2A). The *cyd* gene cluster was separated from the *cox* gene cluster by a 1,656-bp region which contains no functionally assignable ORF and no genetic elements such as CRISPR, tRNA, and rRNA genes. The gene content of *cyd* was similar to that of *cyd* operon in *Bacillus subtilis* (48). The proximity of the *cyd* and *cox* gene clusters (here, the "*cyd–cox* region") raises the possibility that their products might be functionally related to each other.

**Respiratory machineries that can couple with CO oxidation.** We investigated respiratory genes in the G301 genome to estimate the physiological functions of CO oxidation. G301 harbored genes encoding the aerobic respiratory chain, namely, *nuoABCDHIJKLMN* encoding complex I, *sdhABC* encoding complex II, and genes encoding terminal oxidases, such as CydABCD and *cytochrome c* oxidases (Fig. 2B). Regarding anaerobic respiratory machineries, two gene clusters of the respiratory nitrate reductase (*narG1H1I1J1* and *narG2H2I2J2*) were found (Fig. 2B). Both aerobic respiration and nitrate reduction utilize quinones for electron transfer (49, 50). The CO-derived electrons from Mo-CODH may be received by the quinones (51), implying that aerobic respiration and nitrate reduction may be coupled with Mo-CODH-mediated CO oxidation. Quinone-dependent respiratory machinery, except for the aerobic respiratory chain and nitrate reductase, was not identified. In other previously investigated CO oxidizers, the electrons obtained from CO by Ni-CODH are transferred to CooF or ferredoxin for subsequent oxidation-reduction reactions, such as $H_2$ evolution by ECH (52) or $NAD^+$ reduction to NADH by Rnf (53). A lack of any genes homologous to *rnf* suggests that G301 might use ECH to accept electrons from Ni-CODH-mediated CO oxidation. Among the seven known carbon fixation pathways, genes for the reductive glycine pathway (54) are present in the G301 genome. However, these gene products can also function as the glycine cleavage pathway. Therefore, whether they contribute to CO-dependent autotrophic growth in G301 remains unclear.

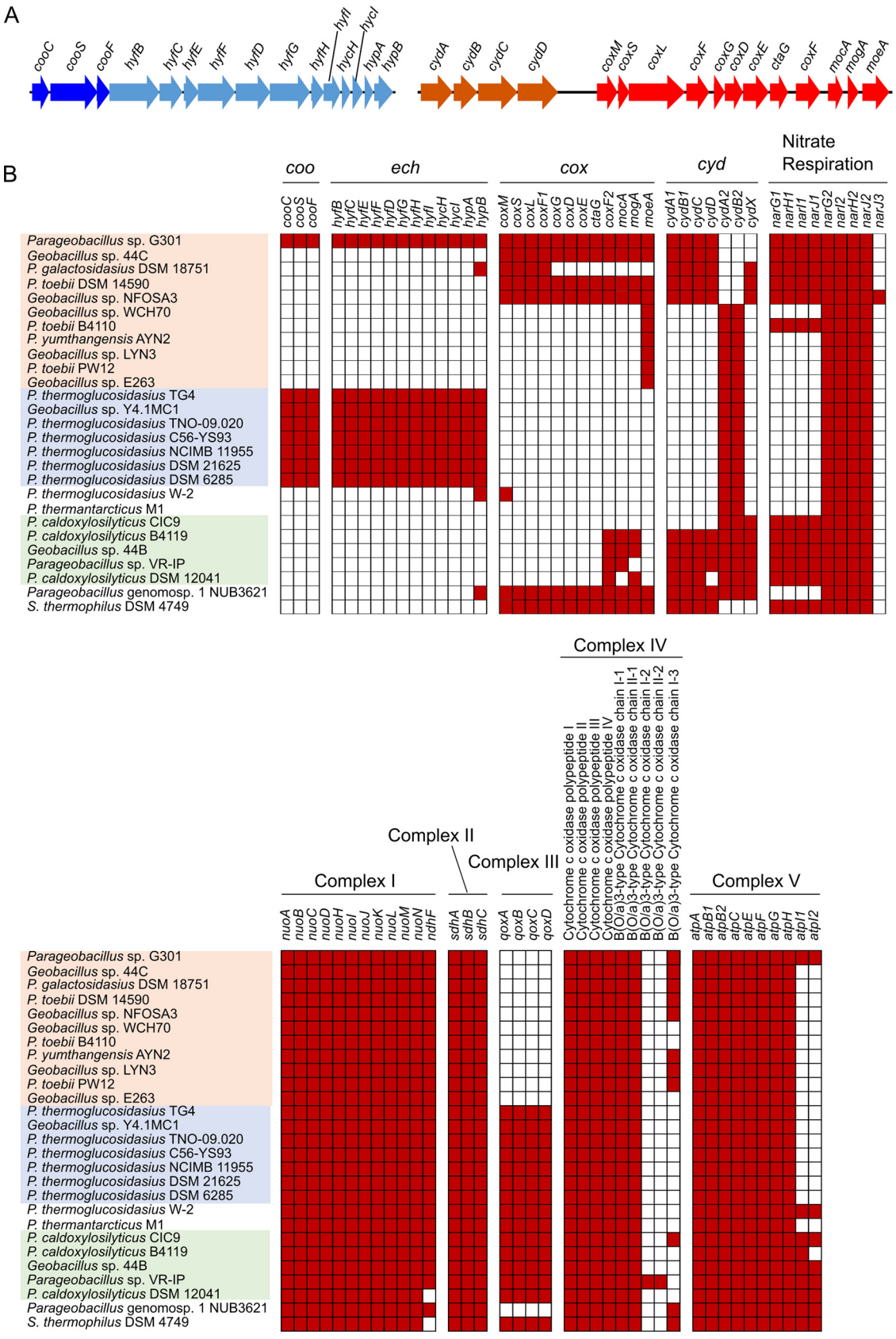


**FIG 2** (A) The organization of the *coo–ech* gene cluster and the *cyd–cox* region of G301. Arrows show coding regions and directions. The *coo*, *ech*, *cox*, and *cyd* gene clusters are colored in blue, light blue, orange, and red, respectively. (B) Summary of

(Continued on next page)

**Distribution of *coo–ech* gene cluster and *cyd–cox* region in *Parageobacillus* genomes.** To explore the distribution of *coo–ech* gene cluster and *cyd–cox* region in the genus *Parageobacillus*, we examined these genes in *Parageobacillus* genomes using OrthoFinder (55) and PATRIC (43).

A single copy of *coo–ech* gene cluster was present in all the genomes which showed an ANI value of ≥95% with *P. thermoglucosidasius* NCIMB 11955, while a single copy of *cyd–cox* region was found in the genomes of *Parageobacillus* genomosp. 1 NUB3621, *S. thermophilus* DSM 4749, *P. toebii* DSM 14590, *Geobacillus* sp. 44C, *Geobacillus* sp. NFOSA3, and *P. galactosidasius* DSM 18751 (Fig. 2B). However, the *cyd–cox* region of *P. galactosidasius* DSM 18751 lacked genes encoding the maturation factors of Cox. No publicly available *Parageobacillus* genomes, other than that of G301, contained both *cooS* and form I *cox*.

To determine whether another prokaryotic isolate could use CO both aerobically and anaerobically, we surveyed *cooS/cdh* and *coxL* against 183,204 prokaryotic isolate genomes in RefSeq/GenBank. While 4,305 and 10,540 isolates harbored *cooS/cdh* and form I/form II *coxL*, respectively, only 6 harbored both genes (Fig. S2A). None of them had both *cooS/cdh* and form I *coxL*, further highlighting the uniqueness of G301 (Fig. S2B).

**Genomic traits shared among *Parageobacillus* strains with *coo–ech* gene cluster or *cyd–cox* region.** The respiratory genes of the G301 genome were broadly distributed among *Parageobacillus* genomes, although there were variations in the presence and absence of homologs (Fig. 2B). There were two sets of genes for aerobic respiratory chain, *cydA* and *cydB*, referred to as *cydA1B1* and *cydA2B2*. The *cydA1B1* genes were located in the *cyd–cox* region (Fig. 2B). The genes for nitrate reduction, *narG1H1I1J1*, were found in 12 genomes, including all of the form I *cox*-containing strains except *Parageobacillus* genomosp. 1 NUB3621. The other gene set for respiratory nitrate reduction, *narG2H2I2J2*, was found in all the *Parageobacillus* genomes (Fig. 2B).

We compared *Parageobacillus* genomes with each other to explore whether the retention of *codh* could affect genomic structures and whether certain cellular functions unrelated to respiration could be coupled with CO oxidation. We first compared the whole-genome synteny among *Parageobacillus* sp. G301, *P. toebii* DSM 14590, and *Geobacillus* sp. WCH70, which were all closely related but have distinct sets of *codh* genes (Fig. 1A and B, Fig. 2B). Genome synteny was highly conserved, indicating that the presence or absence of *coo–ech* gene clusters and *cyd–cox* regions did not result in any unique whole-genome rearrangements (Fig. S3A, B, and C). Subsequently, we compared the synteny of the genomic regions around the *coo–ech* gene cluster and *cyd–cox* region. The genes were conserved in and around the *coo–ech* gene cluster (Fig. S3D) and *cyd–cox* regions, although there were minor differences, such as the translocation or addition of genes in the *cyd–cox* region (Fig. S3E). The genes surrounding the *coo–ech* gene cluster and *cyd–cox* regions were also conserved in *codh*-lacking genomes, indicating that these gene clusters were inserted or deleted in homologous loci without changing the surrounding genomic regions. Finally, we investigated the genes uniquely encoded by genomes with *coo–ech* gene clusters and those with *cyd–cox* regions. Only one gene, except for those in the *coo–ech* gene clusters, was uniquely present in the genomes with *coo–ech* (Fig. 3A). This gene encoded the undecaprenyl-diphosphatase UppP, which contributes to cell wall biosynthesis (56). However, its involvement in hydrogenogenic CO oxidation remains unclear. Conversely, no genes, except for those in the *cox* and *cyd* gene clusters, were uniquely identified in genomes with the *cyd–cox* regions (Fig. 3B).

Overall, the retention of *codh* genes would have a minor effect on genomic structures and cellular functions other than CO-mediated electron transport in *Parageobacillus*.

**CO metabolisms of G301 cultures.** We characterized the CO metabolism of G301 by

**FIG 2** Legend (Continued)
the presence and absence of *codh* and respiratory genes in *Parageobacillus* genomes that can couple with CO oxidation. Top panel: presence and absence of *coo*, *ech*, *cox*, *cyd*, and *nar* genes. Bottom panel: presence and absence of respiratory complex genes other than *cyd*. Strain names are colored in the same manner as in Fig. 1. Detected and undetected genes are filled in as red and white, respectively. Although *hypA* of *Parageobacillus* sp. G301 and *cooF* of *Geobacillus* sp. Y4.1MC1 were not annotated by PATRIC, they were regarded as present because corresponding genes were found in the annotation by DFAST and genomic data obtained from RefSeq, respectively.

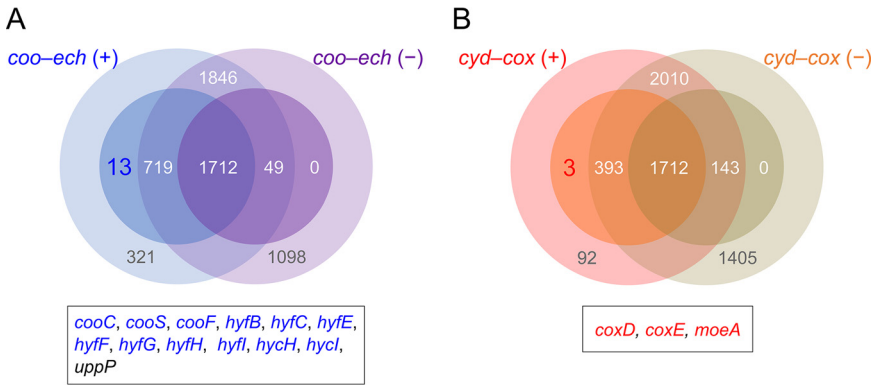


**FIG 3** Comparison of the core and pan-genomes of *Parageobacillus* genomes with and without *codh* gene cluster. (A) Core and pan-genomes of *Parageobacillus* genomes with *coo–ech* gene cluster (*coo–ech* [+]) and without *coo–ech* gene cluster (*coo–ech* [−]). Inner circle represents the core genomes, while outer circle represents the pan-genomes. Numbers indicate shared genes in each category. The category for genes shared exclusively by all the *coo–ech* gene cluster-containing genomes is highlighted, and genes shown in the box are colored blue if they are located in the *coo–ech* gene clusters. (B) Core and pan-genomes of *Parageobacillus* genomes with *cyd–cox* region including accessory genes of *cox* (*cox*, *cyd* [+]) and lacking either or neither of the *cox* and *cyd* gene clusters (*cox*, *cyd* [−]). The category for genes shared exclusively by all the genomes with *cyd–cox* region is highlighted, and those genes shown in the box are colored red if they were located in the *cox* or *cyd* gene clusters. Other details are as described in panel A.

culturing it in medium supplemented with yeast extract as an organic carbon source in the presence or absence of CO and different terminal electron acceptors, i.e., proton, $O_2$, and nitrate. G301 was confirmed to consume CO under all tested conditions (Fig. 4A, D, and G). In the cultures with CO but without $O_2$ and nitrate, CO consumption and $H_2$ and $CO_2$ production were observed from the late log phase to the stationary phase (4 to 24 h after inoculation) (molar ratio of consumed CO/$H_2$ evolved in the gas phase/$CO_2$ evolved in the gas phase = 1:1.03:0.47) (Fig. 4A). Neither $H_2$ nor $CO_2$ production was observed in the culture without CO, $O_2$, and nitrate (Fig. 4B). Although there was no significant increase ($P > 0.05$), the growth yield in the presence of CO was 3.07-fold higher than that without CO (Fig. 4C). CO might have supported growth under these conditions, possibly as an energy source, as indicated in previous studies (21). This result was consistent with that observed in *P. thermoglucosidasius* (41).

In the presence of CO and $O_2$, the consumption of CO and $O_2$ and the production of $CO_2$ were observed until 96 h (molar ratio of consumed CO/consumed $O_2$/$CO_2$ evolved in the gas phase = 1:0.95:0.60), whereas no $H_2$ production was observed (Fig. 4D). The levels of $O_2$ consumed and $CO_2$ evolved in the gas phase at 96 h after inoculation were 32% and 64% lower, respectively, in the culture without CO than in the culture with CO, implying that G301 performed aerobic CO oxidation. Explicit CO depletion was observed during the stationary phase (Fig. 4E), implying that G301 utilized CO as an energy source during starvation as predicted for heterotrophic aerobic CO oxidizers (25). The growth rate in the log phase (0 to 4 h) and growth yield in the culture with CO were not significantly different from those in the culture without CO ($P > 0.05$) (Fig. 4F). However, the depletion of $OD_{600}$ (optical density at 600 nm) during the stationary phase tended to be slower in the culture with CO (Fig. 4F).

In anaerobic cultures with CO and nitrate, complete consumption of CO and nitrate and the production of $CO_2$ and nitrite were observed after 48 h (molar ratio of consumed CO/consumed nitrate/$CO_2$ evolved in the gas phase/nitrite produced = 1:1.79:0.60:1.63). However, $H_2$ production was not observed as in the presence of $O_2$ (Fig. 4G). The amounts of consumed nitrate, $CO_2$ evolved during the gas phase, and nitrite produced at 96 h after inoculation were 46%, 69%, and 40% lower in the absence of CO than in the presence of CO, respectively, indicating the occurrence of CO oxidation coupled with nitrate reduction. Again, explicit CO depletion was observed during the stationary phase (Fig. 4H). The growth rate in the log phase (0 to 4 h) and growth yield in the CO-treated cultures were not significantly different from those in the non-CO-treated cultures ($P > 0.05$). The

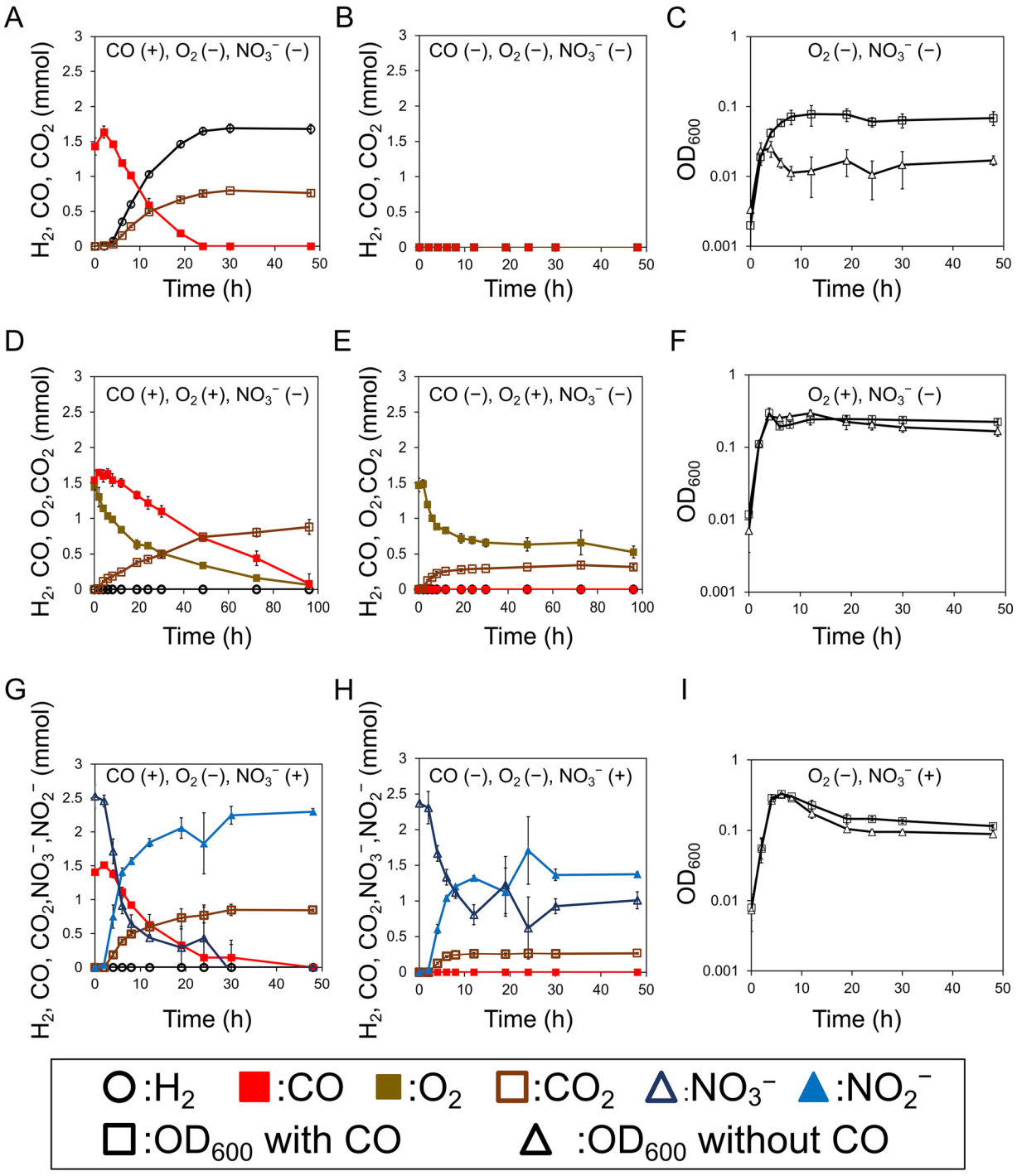


**FIG 4** Growth of the G301 cultures and the levels of CO, $CO_2$, $H_2$, $O_2$, nitrate, and nitrite. The presence and absence of CO, $O_2$, and nitrate under the initial conditions are shown in parentheses in each panel. Plus (+) and minus (−) symbols indicate presence and absence, respectively. (A) Amount of $H_2$, CO, and $CO_2$ in the culture with CO but without $O_2$ and nitrate. (B) Amount of $H_2$, CO, and $CO_2$ in the culture without CO, $O_2$, and nitrate. (C) Growth of cultures under the conditions described in panels A and B. (D) Amount of $O_2$, CO, and $CO_2$ in the culture with CO and $O_2$ but without nitrate. (E) Amount of $O_2$, CO, and $CO_2$ in the culture with $O_2$ but without CO and nitrate. (F) Growth of cultures under the conditions described in panels D and E. (G) Amount of CO, $CO_2$, nitrate, and nitrite in the culture with CO and nitrate but without $O_2$. (H) Amount of CO, $CO_2$, nitrate, and nitrite in the culture with nitrate but without CO and $O_2$. (I) Growth of cultures under the conditions described in panels H and I. Plots represent the means of three biological replicates. Thin vertical lines represent standard deviation.

decrease in $OD_{600}$ in the stationary phase tended to be slower in the presence of CO, as observed in aerobic CO oxidation (Fig. 4I).

To determine which of the CODHs in G301 was responsible for CO oxidation in the presence of nitrate, we examined the CO oxidation of *P. thermoglucosidasius*, which

had a CooS with over 70% amino acid identity to that of G301 but lacked *cox*. *P. thermoglucosidasius* showed CO consumption, $H_2$ production, and $CO_2$ production in cultures with KCl instead of nitrate as the control (Fig. S4A). However, hydrogenogenic CO oxidation was not observed in the nitrate-containing cultures (Fig. S4B), implying that *P. thermoglucosidasius* did not couple nitrate reduction and Ni-CODH-mediated CO oxidation at detectable levels.

## DISCUSSION

Sequencing, *de novo* assembly, and comparative genomic analysis of *Parageobacillus* sp. G301 revealed that this strain was the only isolate with both *cooS/cdh* and form I *cox* (Fig. S2). Cultivation experiments validated the genome-based estimation of CO oxidation in G301, both aerobically and anaerobically (Fig. 4), indicating that both Ni-CODH and Mo-CODH were functional in this strain. In particular, no Ni-CODH-mediated CO oxidation coupled with nitrate reduction was identified in *P. thermoglucosidasius*, indicating that CO oxidation coupled with nitrate reduction in G301 was most likely mediated by Mo-CODH rather than by Ni-CODH, the amino acid sequence of which is highly similar to that of *P. thermoglucosidasius*. Overall, G301 was the only isolate capable of performing CO oxidation coupled with $H_2$ production, $O_2$ reduction, and nitrate reduction. Thus, G301 would conserve energy through CO-mediated respiration under diverse environmental conditions. This metabolic trait may be advantageous in an oxic-anoxic interface because it allows prokaryotes to utilize CO from the atmosphere or other sources such as hydrothermal vents (57), soil (58), seawater (59), or freshwater environments (60, 61) with fluctuating $O_2$ levels. Explorations under such changeable environmental conditions would lead to the discovery of novel CO oxidizers with previously unknown combinations of distinct CO metabolisms, providing further insight into the diversity, evolution, and industrial applications of these prokaryotes with intriguing respiration.

G301 allowed us to further investigate the factors that contributed to the broad but punctate phylogenetic distribution of CO metabolism. Comparative genomic analyses revealed that hydrogenogenic CO oxidation via Ni-CODH, anaerobic CO oxidation coupled with nitrate reduction via Mo-CODH, and aerobic CO oxidation via Mo-CODH showed punctate but not ubiquitous phylogenetic distribution in the genus *Parageobacillus*. The punctate distribution of CO metabolism might be explained by the lack of significant influence of *codh* gene clusters on cellular functions, given that there were no obvious explicit differences in genomes and gene repertoires between CO oxidizers and non-CO oxidizers (Fig. S3). This was consistent with our previous observation that *P. thermoglucosidasius* mutants lacking *codh* could grow with or without CO (41). *codh* genes might act as optional genetic elements that improve fitness under limited conditions rather than as essential genes for cell viability. If this is the case, the gain and loss of *codh* genes may have had less impact on cell physiology and viability. This might result in frequent gain or loss of *codh* genes and may have shaped the current punctate distribution of *codh* genes in the tree of the genus *Parageobacillus*. There are taxa other than *Parageobacillus* which have a punctate distribution of *codh* genes, and CO oxidation does not appear to cause a significant difference in the overall cellular functions. In the family *Roseobacteraceae*, a group of marine bacteria formally known as the Marine Roseobacter Clade, CO oxidizers with form I *cox* gene clusters and non-CO oxidizers without form I *cox* gene clusters are closely related (24). One CO oxidizer of this family, *Ruegeria pomeroyi*, exhibited no observable differences in growth or metabolome between cells grown with and without CO (62), although in a study by Schreier et al. (63), disruption of form I *cox* in this bacterium affected its growth under co-cultivation with multiple bacterial species and a diatom strain. Another example is *Thermoanaerobacter*, a genus of thermophilic anaerobic acetogens. Two anaerobic hydrogenogenic CO oxidizer strains and one strain with the *coo–ech* gene cluster have been characterized, whereas no other strains with *coo–ech* are known (5, 31, 64). One of the two *cooS* genes responsible for hydrogenogenic CO oxidation was deleted in *T. kivui*, a hydrogenogenic CO oxidizer. The resulting mutant lacked the ability to grow on CO, but grew similarly to the parental strain on glucose, mannitol, $H_2+CO_2$, or formate

(65). If the *codh* genes are optional genetic elements, the punctate distribution of *codh* and CO metabolism in various prokaryotic lineages may also be explained, at least partially, as it has for *Parageobacillus*.

## MATERIALS AND METHODS

**Sampling.** Sediment samples were collected from Unagi-ike (31°13′37″ N, 130°36′3″ E) on 12 May 2018. The collected sample was preserved in a 50-mL plastic tube, and the headspace was filled with $N_2$ gas (GL Science Inc., Tokyo, Japan). The sediment was kept under anaerobic conditions by packing it in a freezer bag with Anaero Pack (Mitsubishi Gas Chemical, Tokyo, Japan), cooling it with ice during transportation to the laboratory, and storing it at 4°C until use.

**Isolation.** As liquid medium for enrichment culture, we used a B medium that was modified (41) from the B medium used in a previous study (12); this medium comprised 0.03 g $Na_2SiO_3$, 0.5 g $NH_4Cl$, 0.1 g $KH_2PO_4$, 0.2 g $MgCl_2{\cdot}6H_2O$, 0.1 g $CaCl_2{\cdot}2H_2O$, 0.3 g KCl, 0.1 g $NaHCO_3$, 1 g yeast extract, 0.5 mL trace mineral solution SL-6 (66), and 1 mL vitamin solution (67) per L. For plate cultivation, NBRC 802 agar (42) was used; this medium was composed of 10 g/L hipolypepton, 2 g/L yeast extract, 1 g/L $MgSO_4{\cdot}7H_2O$, and 15 g/L agar. First, 1 g of the sediment was transferred to modified B medium and incubated under a $N_2$:CO (80:20) atmosphere at 65°C in a DRS620DA forced convection oven (Advantec, Tokyo, Japan). The gas composition of the enrichment culture was measured by sampling 1 mL of the gas phase in SVG-3 glass vials (Nichiden Rika-Glass Co., Kobe, Japan) filled with air and sealed with a butyl rubber and melamine cap. Subsequently, the gas (0.5 mL) in the vials was analyzed using a GC-2014 gas chromatography system (Shimadzu, Kyoto, Japan) equipped with a thermal conductivity detector and a Shincarbon ST-packed column (Shinwa Chemical Industries, Kyoto, Japan), using $N_2$ as the carrier gas. When CO consumption and $H_2$ production were observed, the liquid phase of the culture was spread over the NBRC 802 agar plate and incubated at 65°C overnight under aerobic conditions. A single colony was selected and named strain G301. The purity of this isolate was confirmed using Sanger sequencing of the PCR-amplified, partial 16S rRNA gene, as described in the literature (68). A partial 16S rRNA sequence was used as the query for a BLASTn search against the NRBI RefSeq genome database to identify close relatives of G301.

**Observation of cell morphology.** Aerobically grown G301 cells were harvested during the log phase. After fixation by adding glutaraldehyde to a final concentration of 1%, the cells were negatively stained with 2% uranyl acetate (69) and observed under a transmission electron microscope (H-7650; Hitachi, Tokyo, Japan).

**Genome sequencing.** DNA was extracted from G301 cells using a DNeasy Blood & Tissue Kit (Qiagen, Hilden, Germany). The sequence library was prepared using the Nextera Mate Pair Sample Prep kit (Illumina, San Diego, CA, USA) according to the manufacturer's protocol, then sequenced on the MiSeq platform using a MiSeq Reagent Kit v3 (2 × 300 bp paired-end) (Illumina, San Diego, CA, USA), yielding 3,272,078 paired-end reads. Quality trimming and adapter removal were performed with Trimmomatic v.0.3.6 (70) by setting the "ILLUMINACLIP" option at 2:30:10, "LEADING" and "TRAILING" options at 3, "SLIDINGWINDOW" option at 4:15, and "MINLEN" option at 30. Further trimming of mate-pair adapter sequences was performed using NxTrim v.0.4.1 (71) with default parameters, resulting in 2,769,352 paired-end reads. The qualified paired-end reads were assembled with SPAdes v.3.13.0 using the "-hqmp" and "-careful" options (72). Mate pair sequences were mapped against the assembled contigs using Burrows-Wheeler Aligner (BWA) v.0.7.17 (73) and SAMtools v.0.1.19 (74) with default parameters, and the quality of the assembled scaffolds was evaluated using NxRepair v.0.13 (75). The draft genome was annotated using DFAST v.1.2.6 (46).

**Phylogenetic analysis of *Parageobacillus* isolates.** The genome sequences of G301 and *Parageobacillus* strains retrieved from NCBI RefSeq (76), GTDB (77), and PATRIC (43) were subjected to an all-versus-all comparison of ANI using FastANI (45) with default parameters. Genome pairs that showed an ANI above 99.9% were regarded as identical, and one of the genomes was removed at this step. The genome size, GC content, and number of scaffolds of the remaining genomes were evaluated with quast v.5.0.2 (78). The number of protein-coding genes was estimated using PATRIC (43).

To determine the phylogenetic position of G301, 16S rRNA gene sequences were retrieved from 18 *Parageobacillus* genomes and the genome of *G. thermodenitrificans* NG80-2 as an outgroup. Sequences were aligned using the L-INS-I method in MAFFT (79) v.7.471 and trimmed using trimAl v.1.4.1 (80) with the "automated1" option, resulting in a data set of 19 taxa and 1,562 sites. The maximum-likelihood tree was reconstructed using IQTREE v.1.6.12 (81) under the TN+F+R2 model, which was selected as the best model based on the BIC for the data set, with 1,000 ultrafast bootstrap analyses. The tree was visualized using the Interactive Tree Of Life (iTOL) web server (82). We determined the phylogenetic relationships among *Parageobacillus* strains based on core protein-coding genes, which were single-copy genes present in all 27 *Parageobacillus* and *G. thermodenitrificans* genomes. All encoded proteins, including hypothetical proteins, were clustered using OrthoFinder v.2.5.2 (55). The translated amino acid sequences of the identified 1,505 core genes in the 28 genomes were aligned using muscle v.3.8.31 (83) with the default parameters, trimmed using trimAl v.1.4.1 (80), and concatenated to yield a data set of 28 taxa and 421,717 sites. The maximum-likelihood tree was reconstructed using IQTREE v.1.6.12 (81) under the JTT+F+R4 substitution model, which was selected as the best model based on the BIC for the data set, with 100 bootstrap analyses. The tree was visualized as previously described.

**Identification of genomes with *codh* from *Parageobacillus* isolates and from the NCBI genome database.** Using CooS of *P. thermoglucosidasius* strain TG4 as a cue, homologs of *cooS* in the analyzed genomes were identified using OrthoFinder v.2.5.2 (55). The obtained protein sequences were confirmed to be CooS using phylogenetic analysis, followed by a comparison of the active-site motifs. We constructed a phylogenetic tree with amino acid sequences of CooS homologs with representative CooS sequences of

each clade from A to G, as well as mini-CooS (16) (WP_011305243.1, WP_026514536.1, WP_039226206.1, WP_011342982.1, WP_012571978.1, WP_011343033.1, OGP75751.1, and WP_007288589.1, respectively), mentioned in the previous study (14), and hydroxylamine reductase (WP_010939296.1) as the outgroup. These sequences were aligned and trimmed as described above for the phylogenetic analysis of 16S rRNA, resulting in a data set of 17 taxa and 613 sites. The data set was subjected to maximum-likelihood analysis with IQTREE v.1.6.12 (81) under the Blosum62+G4 model, which was automatically selected as the best model based on the BIC for the data set, with 1,000 ultrafast bootstrap analyses. The tree was visualized as previously described. To identify the active site motif of CooS homologs, alignment was visualized using MEGA-X (84), and the presence of the conserved catalytic site and surrounding metal clusters, as previously described (14), was manually checked.

Homologs of CoxL were identified as described for CooS, using CoxL from *P. toebii* strain DSM 14590 as a query. In contrast to CooS, CoxL homologs may contain different proteins of the xanthine oxidase family (85). We performed a phylogenetic analysis, followed by a comparison of the active site motifs to remove proteins other than form I CoxL. We compared all detected CoxL homologs with the form I CoxL sequences of *Afipia carboxidovorans* and *Mycobacterium tuberculosis* (1ZXI_2 and SRX92445.1, respectively), both of which oxidize CO in cultivation experiments (86, 87). Enzymatic analysis of *A. carboxidovorans* confirmed CO oxidation by the form I CoxL (51). Sequences were aligned and trimmed as described above, resulting in a data set of 15 taxa and 819 sites. The data set was subjected to maximum-likelihood analysis using IQTREE v.1.6.12 (81) under the LG+I+G4 model, which was automatically selected as the best model based on the BIC for the data set, with 1,000 ultrafast bootstrap analyses. The tree was visualized as described previously. The alignment was visualized using MEGA-X (84), and AYXCSFR, the motif of the active site of functional form I CoxL, as reported in a previous study (3), was manually checked. We removed six proteins that were found in *Parageobacillus* genomes but did not conserve the active site motif and formed a different group from the known form I CoxL on the phylogenetic tree (Fig. S5).

Genomes containing both *cooS/cdh* and form I *coxL* were also explored for available genomes as described in our previous study (17). Briefly, CooS/Cdh was searched using the BLASTp of DIAMOND v.0.9.29 (88) against the NCBI non-redundant protein database (February 2020) using representative sequences from clades A to G of CooS/Cdh and mini-CooS as queries. Sequences with an E value of $<0.001$, $\geq 400$ amino acids, and including the conserved catalytic site and the surrounding metal clusters described previously (14) were regarded as genuine CooS/Cdh. To identify genomes with form I *coxL*, we searched for genomes carrying *coxL* homologs by BLASTp search using DIAMOND v.0.9.29, using the amino acid sequence of form I CoxL of *A. carboxidovorans* (1ZXI_2) as a query. Sequences with E values of $<0.001$, $\geq 400$ amino acids, and bit scores of $\geq 500$ were obtained regardless of whether they had the active site motif of form I CoxL. Genomes containing *cooS/cdh* and *coxL* were obtained from the RefSeq/GenBank genome database as described by Omae et al. (31). CoxL homologs encoded in the genomes of CooS homologs were classified as form I CoxL or other proteins, as described above.

**Comparative genomic analysis.** To analyze the genomic context of *cooS* and form I *coxL* and to explore the conservation of respiratory machinery, protein-coding genes in the *Parageobacillus* genomes were predicted and re-annotated with PATRIC v.3.6.8 and a BLASTp search against the NCBI non-redundant protein database. Whole-genome synteny was evaluated using the nucmer method in MUMmer v.3.23 (89). To analyze the conservation of genomic regions around Ni-CODH/Mo-CODH, the genomic regions around *coo–ech* and *cox–cyd* were annotated using the RAST server v.2.0 (90) and a BLASTx search against NCBI non-redundant protein sequences. The conservation of genomic regions was visualized using EasyFig v.2.2.3 (91). Additionally, if we found a long noncoding region, we searched for genetic elements such as CRISPR and RNA genes using CRT (CRISPR Recognition Tool) v.1.1 (92), tRNAscan-SE v.2.0 (93), and RNAmmer v.1.2 (94). The conservation of regions surrounding *coo–ech* was examined by comparing genomes bearing *coo–ech* with each other and with strains lacking *coo–ech* (*P. toebii* DSM 14590 for *Parageobacillus* sp. G301, and *P. thermoglucosidasius* W-2 for *P. thermoglucosidasius* TG4). Conservation around the *cyd–cox* region was analyzed by comparing genomes bearing the *cyd–cox* region with each other and with strains lacking *cyd–cox* region (*P. caldoxylosilyticus* ClC9 for *Parageobacillus* genomosp. 1 NUB3621, and *Geobacillus* sp. E263 for *P. galactosidasius* DSM 18751). To investigate the cell functions conserved in genomes with *codh*, the presence or absence of the orthologous genes identified above using OrthoFinder was compared between genomes with and without the *coo–ech* gene cluster and between genomes with *cyd–cox* region containing accessory genes of *cox* and genomes without one.

**Cultivation in the presence of different terminal electron acceptors.** G301 cells were cultured with and without CO as follows: frozen stock of G301 was streaked on TGP agar (95) and incubated overnight at 65°C under aerobic conditions. A single colony was injected into 5 mL of modified B medium in a 180 × 18-mm glass test tube (IWAKI, Tokyo, Japan) with a polycarbonate screw cap (IWAKI, Tokyo, Japan) and grown aerobically at 65°C and pH 6.7. Growth was monitored by measuring the $OD_{600}$ of the culture using an Ultrospec2100 (Biochrom, Cambridge, UK). When the $OD_{600}$ reached 0.49 to 0.56, around the exponential growth phase, a 500-$\mu$L aliquot was injected into 50 mL of modified B medium in 300-mL glass bottles (PYREX, Osaka, Japan) sealed with bromobutyl rubber stoppers (Altair Corporation, Yokohama, Japan) and phenol resin screw caps (SIBATA, Tokyo, Japan).

To characterize CO metabolism, G301 cells were cultured under three distinct conditions. G301 was cultured with neither $O_2$ nor nitrate in the modified B medium described above under a $N_2$:CO (80:20) atmosphere or a 100% $N_2$ atmosphere as a negative control at 65°C and pH 6.8 with gyratory shaking at 100 rpm. Growth was monitored by measuring the $OD_{600}$. The gas composition was monitored as described above and Ar was used as the carrier gas.

G301 was cultured under an $N_2$:CO (80:20) atmosphere or 100% $N_2$ atmosphere as a negative control, as described above, with the exception of modified B medium including 5.0 g/L $KNO_3$. The growth and gas

composition were monitored as described above. Nitrate and nitrite were quantified by the Griess reaction using a $NO_2/NO_3$ Assay Kit CII (Dojindo Laboratories, Kumamoto, Japan) according to the manufacturer's protocol.

G301 cells were cultured in an air:CO (80:20) or air:$N_2$ (80:20) atmosphere as a negative control at 65°C and pH 6.7 with gyratory shaking at 100 rpm. Growth and gas composition were monitored as described above, except that the gas vials were purged with Ar to quantify $O_2$ prior to analysis. Each experiment was conducted in triplicates. The significance of differences in growth yield and growth rate was analyzed using Welch's *t* test.

To analyze whether *Parageobacillus* with only *cooS* can couple CO oxidation with nitrate reduction, we cultured *P. thermoglucosidasius* in $N_2$:CO (75:25) atmosphere in the presence and absence of nitrate ($KNO_3$ or KCl was added at a final concentration of 50 mM, respectively) at 65°C and pH 7.0. We used Bly medium, which has a composition similar to that of the modified B medium; however, the amount of yeast extract was reduced by one-tenth.

**Data availability.** The genome of strain G301 was deposited in GenBank under the name "BioProject PRJDB14871" (accession numbers for each scaffold are BSDB01000001 to BSDB01000009; BioSample SAMD00562293).

## SUPPLEMENTAL MATERIAL

Supplemental material is available online only.

**SUPPLEMENTAL FILE 1**, XLSB file, 6.1 MB.

**SUPPLEMENTAL FILE 2**, XLSX file, 0.02 MB.

**SUPPLEMENTAL FILE 3**, XLSX file, 0.6 MB.

**SUPPLEMENTAL FILE 4**, PDF file, 0.7 MB.

## ACKNOWLEDGMENTS

This work was supported by JSPS KAKENHI grant no. JP16H06381 (to Y.S.) and the Institute for Fermentation, Osaka (grant L-2021-1-002 to T.Y.). Computation time was provided by the SuperComputer System, Institute for Chemical Research, Kyoto University.

We thank Editage (www.editage.com) for English language editing.

## REFERENCES

1. Chin BY, Otterbein LE. 2009. Carbon monoxide is a poison. . . to microbes! CO as a bactericidal molecule. Curr Opin Pharmacol 9:490–500. https://doi.org/10.1016/j.coph.2009.06.025.
2. Coburn RF. 1979. Mechanisms of carbon monoxide toxicity. Prev Med 8:310–322. https://doi.org/10.1016/0091-7435(79)90008-2.
3. King GM, Weber CF. 2007. Distribution, diversity and ecology of aerobic CO-oxidizing bacteria. Nat Rev Microbiol 5:107–118. https://doi.org/10.1038/nrmicro1595.
4. Slobodkin A, Slobodkina G, Allioux M, Alain K, Jebbar M, Shadrin V, Kublanov I, Toshchakov S, Bonch-Osmolovskaya E. 2019. Genomic insights into the carbon and energy metabolism of a thermophilic deep-sea bacterium *Deferribacter autotrophicus* revealed new metabolic traits in the phylum *Deferribacteres*. Genes 10:849. https://doi.org/10.3390/genes10110849.
5. Weghoff MC, Müller V. 2016. CO metabolism in the thermophilic acetogen *Thermoanaerobacter kivui*. Appl Environ Microbiol 82:2312–2319. https://doi.org/10.1128/AEM.00122-16.
6. Yoneda Y, Yoshida T, Yasuda H, Imada C, Sako Y. 2013. A thermophilic, hydrogenogenic and carboxydotrophic bacterium, *Calderihabitans maritimus* gen. nov., sp. nov., from a marine sediment core of an undersea caldera. Int J Syst Evol Microbiol 63:3602–3608. https://doi.org/10.1099/ijs.0.050468-0.
7. Fukuyama Y, Inoue M, Omae K, Yoshida T, Sako Y. 2020. Anaerobic and hydrogenogenic carbon monoxide-oxidizing prokaryotes: versatile microbial conversion of a toxic gas into an available energy. Adv Appl Microbiol 110:99–148. https://doi.org/10.1016/bs.aambs.2019.12.001.
8. Thauer RK. 1990. Energy metabolism of methanogenic bacteria. Biochim Biophys Acta Bioenerg 1018:256–259. https://doi.org/10.1016/0005-2728(90)90261-2.
9. King GM. 2006. Nitrate-dependent anaerobic carbon monoxide oxidation by aerobic CO-oxidizing bacteria. FEMS Microbiol Ecol 56:1–7. https://doi.org/10.1111/j.1574-6941.2006.00065.x.
10. Myers M, King GM. 2017. Perchlorate-coupled carbon monoxide (CO) oxidation: evidence for a plausible microbe-mediated reaction in Martian brines. Front Microbiol 8:2571. https://doi.org/10.3389/fmicb.2017.02571.
11. Robb FT, Techtmann SM. 2018. Life on the fringe: microbial adaptation to growth on carbon monoxide. F1000Res 7:1981. https://doi.org/10.12688/f1000research.16059.1.
12. Yoneda Y, Yoshida T, Kawaichi S, Daifuku T, Takabe K, Sako Y. 2012. *Carboxydothermus pertinax* sp. nov., a thermophilic, hydrogenogenic, Fe(III)-reducing, sulfur-reducing carboxydotrophic bacterium from an acidic hot spring. Int J Syst Evol Microbiol 62:1692–1697. https://doi.org/10.1099/ijs.0.031583-0.
13. Techtmann SM, Colman AS, Robb FT. 2009. 'That which does not kill us only makes us stronger': the role of carbon monoxide in thermophilic microbial consortia. Environ Microbiol 11:1027–1037. https://doi.org/10.1111/j.1462-2920.2009.01865.x.
14. Inoue M, Nakamoto I, Omae K, Oguro T, Ogata H, Yoshida T, Sako Y. 2018. Structural and phylogenetic diversity of anaerobic carbon-monoxide dehydrogenases. Front Microbiol 9:3353. https://doi.org/10.3389/fmicb.2018.03353.
15. Dobbek H, Gremer L, Meyer O, Huber R. 1999. Crystal structure and mechanism of CO dehydrogenase, a molybdo iron-sulfur flavoprotein containing *S*-selanylcysteine. Proc Natl Acad Sci U S A 96:8884–8889. https://doi.org/10.1073/pnas.96.16.8884.
16. Techtmann SM, Lebedinsky AV, Colman AS, Sokolova TG, Woyke T, Goodwin L, Robb FT. 2012. Evidence for horizontal gene transfer of anaerobic carbon monoxide dehydrogenases. Front Microbiol 3:132. https://doi.org/10.3389/fmicb.2012.00132.
17. Inoue M, Omae K, Nakamoto I, Kamikawa R, Yoshida T, Sako Y. 2022. Biome-specific distribution of Ni-containing carbon monoxide dehydrogenases. Extremophiles 26:9. https://doi.org/10.1007/s00792-022-01259-y.
18. Ensign SA, Ludden PW. 1991. Characterization of the CO oxidation/$H_2$ evolution system of *Rhodospirillum rubrum*. Role of a 22-kDa iron-sulfur protein in mediating electron transfer between carbon monoxide dehydrogenase and hydrogenase. J Biol Chem 266:18395–18403. https://doi.org/10.1016/S0021-9258(18)55283-2.
19. Jeon WB, Cheng J, Ludden PW. 2001. Purification and characterization of membrane-associated CooC protein and its functional role in the insertion of nickel into carbon monoxide dehydrogenase from *Rhodospirillum rubrum*. J Biol Chem 276:38602–38609. https://doi.org/10.1074/jbc.M104945200.
20. Singer SW, Hirst MB, Ludden PW. 2006. CO-dependent $H_2$ evolution by *Rhodospirillum rubrum*: role of CODH:CooF complex. Biochim Biophys Acta 1757:1582–1591. https://doi.org/10.1016/j.bbabio.2006.10.003.
21. Schoelmerich MC, Müller V. 2019. Energy conservation by a hydrogenase-dependent chemiosmotic mechanism in an ancient metabolic pathway.

Proc Natl Acad Sci U S A 116:6329–6334. https://doi.org/10.1073/pnas.1818580116.
22. Schut GJ, Lipscomb GL, Nguyen DMN, Kelly RM, Adams MWW. 2016. Heterologous production of an energy-conserving carbon monoxide dehydrogenase complex in the hyperthermophile *Pyrococcus furiosus*. Front Microbiol 7:29. https://doi.org/10.3389/fmicb.2016.00029.
23. King GM. 2003. Molecular and culture-based analyses of aerobic carbon monoxide oxidizer diversity. Appl Environ Microbiol 69:7257–7265. https://doi.org/10.1128/AEM.69.12.7257-7265.2003.
24. Cunliffe M. 2011. Correlating carbon monoxide oxidation with *cox* genes in the abundant Marine Roseobacter Clade. ISME J 5:685–691. https://doi.org/10.1038/ismej.2010.170.
25. Cordero PRF, Bayly K, Man Leung P, Huang C, Islam ZF, Schittenhelm RB, King GM, Greening C. 2019. Atmospheric carbon monoxide oxidation is a widespread mechanism supporting microbial survival. ISME J 13:2868–2881. https://doi.org/10.1038/s41396-019-0479-8.
26. Cypionka H, Verseveld HW, Stouthamer AH. 1984. Proton translocation coupled to carbon monoxide-insensitive and -sensitive electron transport in *Pseudomonas carboxydovorans*. FEMS Microbiol Lett 22:209–213. https://doi.org/10.1111/j.1574-6968.1984.tb00728.x.
27. Nanba K, King GM, Dunfield K. 2004. Analysis of facultative lithotroph distribution and diversity on volcanic deposits by use of the large subunit of ribulose 1,5-bisphosphate carboxylase/oxygenase. Appl Environ Microbiol 70:2245–2253. https://doi.org/10.1128/AEM.70.4.2245-2253.2004.
28. Santiago B, Schübel U, Egelseer C, Meyer O. 1999. Sequence analysis, characterization and CO-specific transcription of the *cox* gene cluster on the megaplasmid pHCG3 of *Oligotropha carboxidovorans*. Gene 236:115–124. https://doi.org/10.1016/s0378-1119(99)00245-0.
29. Merrouch M, Hadj-Saïd J, Domnik L, Dobbek H, Léger C, Dementin S, Fourmond V. 2015. $O_2$ inhibition of Ni-containing CO dehydrogenase is partly reversible. Chemistry 21:18934–18938. https://doi.org/10.1002/chem.201502835.
30. Sokolova TG, Yakimov MM, Chernyh NA, Lun'kova E, Kostrikina NA, Taranov EA, Lebedinskii AV, Bonch-Osmolovskaya EA. 2017. Aerobic carbon monoxide oxidation in the course of growth of a hyperthermophilic archaeon, *Sulfolobus* sp. ETSY. Microbiology 86:539–548. https://doi.org/10.1134/S0026261717050174.
31. Omae K, Fukuyama Y, Yasuda H, Mise K, Yoshida T, Sako Y. 2019. Diversity and distribution of thermophilic hydrogenogenic carboxydotrophs revealed by microbial community analysis in sediments from multiple hydrothermal environments in Japan. Arch Microbiol 201:969–982. https://doi.org/10.1007/s00203-019-01661-9.
32. Artuso I, Turrini P, Pirolo M, Lucidi M, Tescari M, Visaggio D, Mansi A, Lugli GA, Ventura M, Visca P. 2021. Phylogenomic analysis and characterization of carbon monoxide utilization genes in the family *Phyllobacteriaceae* with reclassification of *Aminobacter carboxidus* (Meyer et al. 1993, Hördt et al. 2020) as *Aminobacter lissarensis* comb. nov. (McDonald et al. 2005). Syst Appl Microbiol 44:126199. https://doi.org/10.1016/j.syapm.2021.126199.
33. Coorevits A, Dinsdale AE, Halket G, Lebbe L, De Vos P, Van Landschoot A, Logan NA. 2012. Taxonomic revision of the genus *Geobacillus*: emendation of *Geobacillus*, *G. stearothermophilus*, *G. jurassicus*, *G. toebii*, *G. thermodenitrificans* and *G. thermoglucosidans* (nom. corrig., formerly '*thermoglucosidasius*'); transfer of *Bacillus thermantarcticus* to the genus as *G. thermantarcticus* comb. nov.; proposal of *Caldibacillus debilis* gen. nov., comb. nov.; transfer of *G. tepidamans* to *Anoxybacillus* as *A. tepidamans* comb. nov.; and proposal of *Anoxybacillus caldiproteolyticus* sp. nov. Int J Syst Evol Microbiol 62:1470–1485. https://doi.org/10.1099/ijs.0.030346-0.
34. Aliyu H, Lebre P, Blom J, Cowan D, De Maayer P. 2016. Phylogenomic re-assessment of the thermophilic genus *Geobacillus*. Syst Appl Microbiol 39:527–533. https://doi.org/10.1016/j.syapm.2016.09.004.
35. Aliyu H, Lebre P, Blom J, Cowan D, De Maayer P. 2018. Corrigendum to "Phylogenomic re-assessment of the thermophilic genus *Geobacillus*" [Syst. Appl. Microbiol. 39 (2016) 527–533]. Syst Appl Microbiol 41:529–530. https://doi.org/10.1016/j.syapm.2018.07.001.
36. Najar IN, Thakur N. 2020. A systematic review of the genera *Geobacillus* and *Parageobacillus*: their evolution, current taxonomic status and major applications. Microbiology (Reading) 166:800–816. https://doi.org/10.1099/mic.0.000945.
37. Madhaiyan M, Saravanan VS, See-Too W-S. 2020. Genome based analyses reveals the presence of heterotypic synonyms and subspecies in *Bacteria* and *Archaea*. bioRxiv. https://doi.org/10.1101/2020.12.13.418756.
38. Mohr T, Aliyu H, Küchlin R, Polliack S, Zwick M, Neumann A, Cowan D, de Maayer P. 2018. CO-dependent hydrogen production by the facultative anaerobe *Parageobacillus thermoglucosidasius*. Microb Cell Fact 17:108. https://doi.org/10.1186/s12934-018-0954-3.
39. Mohr T, Aliyu H, Küchlin R, Zwick M, Cowan D, Neumann A, de Maayer P. 2018. Comparative genomic analysis of *Parageobacillus thermoglucosidasius* strains with distinct hydrogenogenic capacities. BMC Genomics 19:880. https://doi.org/10.1186/s12864-018-5302-9.
40. Inoue M, Tanimura A, Ogami Y, Hino T, Okunishi S, Maeda H, Yoshida T, Sako Y. 2019. Draft genome sequence of *Parageobacillus thermoglucosidasius* strain TG4, a hydrogenogenic carboxydotrophic bacterium isolated from a marine sediment. Microbiol Resour Announc 8:e01666-18. https://doi.org/10.1128/MRA.01666-18.
41. Adachi Y. 2021. Genetic engineering of carbon monoxide-dependent hydrogen-producing machinery in *Parageobacillus thermoglucosidasius*. Microbes Environ 35:ME20101.
42. Yamamura H, Hayashi T, Hamada M, Kohda T, Serisawa Y, Matsuyama-Serisawa K, Nakagawa Y, Otoguro M, Yanagida F, Tamura T, Hayakawa M. 2019. *Cellulomonas algicola* sp. nov., an actinobacterium isolated from a freshwater alga. Int J Syst Evol Microbiol 69:2723–2728. https://doi.org/10.1099/ijsem.0.003549.
43. Wattam AR, Davis JJ, Assaf R, Boisvert S, Brettin T, Bun C, Conrad N, Dietrich EM, Disz T, Gabbard JL, Gerdes S, Henry CS, Kenyon RW, Machi D, Mao C, Nordberg EK, Olsen GJ, Murphy-Olson DE, Olson R, Overbeek R, Parrello B, Pusch GD, Shukla M, Vonstein V, Warren A, Xia F, Yoo H, Stevens RL. 2017. Improvements to PATRIC, the all-bacterial Bioinformatics Database and Analysis Resource Center. Nucleic Acids Res 45:D535–D542. https://doi.org/10.1093/nar/gkw1017.
44. Schoch CL, Ciufo S, Domrachev M, Hotton CL, Kannan S, Khovanskaya R, Leipe D, Mcveigh R, O'Neill K, Robbertse B, Sharma S, Soussov V, Sullivan JP, Sun L, Turner S, Karsch-Mizrachi I. 2020. NCBI Taxonomy: a comprehensive update on curation, resources and tools. Database 2020:baaa062. https://doi.org/10.1093/database/baaa062.
45. Jain C, Rodriguez-R LM, Phillippy AM, Konstantinidis KT, Aluru S. 2018. High throughput ANI analysis of 90K prokaryotic genomes reveals clear species boundaries. Nat Commun 9:5114. https://doi.org/10.1038/s41467-018-07641-9.
46. Tanizawa Y, Fujisawa T, Nakamura Y. 2018. DFAST: a flexible prokaryotic genome annotation pipeline for faster genome publication. Bioinformatics 34:1037–1039. https://doi.org/10.1093/bioinformatics/btx713.
47. Søndergaard D, Pedersen CNS, Greening C. 2016. HydDB: a web tool for hydrogenase classification and analysis. Sci Rep 6:34212. https://doi.org/10.1038/srep34212.
48. Winstedt L, Yoshida K-I, Fujita Y, von Wachenfeldt C. 1998. Cytochrome bd biosynthesis in *Bacillus subtilis*: characterization of the *cydABCD* operon. J Bacteriol 180:6571–6580. https://doi.org/10.1128/JB.180.24.6571-6580.1998.
49. Magalon A, Fedor JG, Walburger A, Weiner JH. 2011. Molybdenum enzymes in bacteria and their maturation. Coord Chem Rev 255:1159–1178. https://doi.org/10.1016/j.ccr.2010.12.031.
50. Sharma P, Teixeira de Mattos MJ, Hellingwerf KJ, Bekker M. 2012. On the function of the various quinone species in *Escherichia coli*. FEBS J 279:3364–3373. https://doi.org/10.1111/j.1742-4658.2012.08608.x.
51. Wilcoxen J, Zhang B, Hille R. 2011. Reaction of the molybdenum- and copper-containing carbon monoxide dehydrogenase from *Oligotropha carboxydovorans* with quinones. Biochemistry 50:1910–1916. https://doi.org/10.1021/bi1017182.
52. Soboh B, Linder D, Hedderich R. 2002. Purification and catalytic properties of a CO-oxidizing:$H_2$-evolving enzyme complex from *Carboxydothermus hydrogenoformans*. Eur J Biochem 269:5712–5721. https://doi.org/10.1046/j.1432-1033.2002.03282.x.
53. Wiechmann A, Trifunović D, Klein S, Müller V. 2020. Homologous production, one-step purification, and proof of $Na^+$ transport by the Rnf complex from *Acetobacterium woodii*, a model for acetogenic conversion of C1 substrates to biofuels. Biotechnol Biofuels 13:208. https://doi.org/10.1186/s13068-020-01851-4.
54. Sánchez-Andrea I, Guedes IA, Hornung B, Boeren S, Lawson CE, Sousa DZ, Bar-Even A, Claassens NJ, Stams AJM. 2020. The reductive glycine pathway allows autotrophic growth of *Desulfovibrio desulfuricans*. Nat Commun 11:5090. https://doi.org/10.1038/s41467-020-18906-7.
55. Emms DM, Kelly S. 2019. OrthoFinder: phylogenetic orthology inference for comparative genomics. Genome Biol 20:238. https://doi.org/10.1186/s13059-019-1832-y.
56. Ghachi ME, Bouhss A, Blanot D, Mengin-Lecreulx D. 2004. The *bacA* gene of *Escherichia coli* encodes an undecaprenyl pyrophosphate phosphatase activity. J Biol Chem 279:30106–30113. https://doi.org/10.1074/jbc.M401701200.
57. Chiodini G, Caliro S, Caramanna G, Granieri D, Minopoli C, Moretti R, Perotta L, Ventura G. 2006. Geochemistry of the submarine gaseous emissions of Panarea (Aeolian islands, southern Italy): magmatic vs. hydrothermal origin

and implications for volcanic surveillance. Pure Appl Geophys 163:759–780. https://doi.org/10.1007/s00024-006-0037-y.
58. Schade GW, Crutzen PJ. 1999. CO emissions from degrading plant matter (II). Tellus B Chem Phys Meteorol 51:909–918. https://doi.org/10.3402/tellusb.v51i5.16503.
59. Conte L, Szopa S, Séférian R, Bopp L. 2019. The oceanic cycle of carbon monoxide and its emissions to the atmosphere. Biogeosciences 16:881–902. https://doi.org/10.5194/bg-16-881-2019.
60. Zuo Y, Jones RD. 1997. Photochemistry of natural dissolved organic matter in lake and wetland waters: production of carbon monoxide. Water Res 31:850–858. https://doi.org/10.1016/S0043-1354(96)00316-8.
61. Montag D, Schink B. 2018. Formate and hydrogen as electron shuttles in terminal fermentations in an oligotrophic freshwater lake sediment. Appl Environ Microbiol 84:e01572-18. https://doi.org/10.1128/AEM.01572-18.
62. Cunliffe M. 2013. Physiological and metabolic effects of carbon monoxide oxidation in the model marine bacterioplankton *Ruegeria pomeroyi* DSS-3. Appl Environ Microbiol 79:738–740. https://doi.org/10.1128/AEM.02466-12.
63. Schreier JE, Smith CB, Ioerger TR, Moran MA. 2023. A mutant fitness assay identifies bacterial interactions in a model ocean hot spot. Proc Natl Acad Sci U S A 120:e2217200120. https://doi.org/10.1073/pnas.2217200120.
64. Balk M, Heilig HGHJ, van Eekert MHA, Stams AJM, Rijpstra IC, Sinninghe-Damsté JS, de Vos WM, Kengen SWM. 2009. Isolation and characterization of a new CO-utilizing strain, *Thermoanaerobacter thermohydrosulfuricus* subsp. *carboxydovorans*, isolated from a geothermal spring in Turkey. Extremophiles 13:885–894. https://doi.org/10.1007/s00792-009-0276-9.
65. Jain S, Katsyv A, Basen M, Müller V. 2021. The monofunctional CO dehydrogenase CooS is essential for growth of *Thermoanaerobacter kivui* on carbon monoxide. Extremophiles 26:4. https://doi.org/10.1007/s00792-021-01251-y.
66. Pfennig N. 1974. *Rhodopseudomonas globiformis*, sp. n., a new species of the *Rhodospirillaceae*. Arch Microbiol 100:197–206. https://doi.org/10.1007/BF00446317.
67. Wolin EA, Wolin MJ, Wolfe RS. 1963. Formation of methane by bacterial extracts. J Biol Chem 238:2882–2886. https://doi.org/10.1016/S0021-9258(18)67912-8.
68. Fukuyama Y, Tanimura A, Inoue M, Omae K, Yoshida T, Sako Y. 2019. Draft genome sequences of two thermophilic *Moorella* sp. strains, isolated from an acidic hot spring in Japan. Microbiol Resour Announc 8:e00663-19. https://doi.org/10.1128/MRA.00663-19.
69. Watson ML. 1958. Staining of tissue sections for electron microscopy with heavy metals. J Biophys Biochem Cytol 4:475–478. https://doi.org/10.1083/jcb.4.4.475.
70. Bolger AM, Lohse M, Usadel B. 2014. Trimmomatic: a flexible trimmer for Illumina sequence data. Bioinformatics 30:2114–2120. https://doi.org/10.1093/bioinformatics/btu170.
71. O'Connell J, Schulz-Trieglaff O, Carlson E, Hims MM, Gormley NA, Cox AJ. 2015. NxTrim: optimized trimming of Illumina mate pair reads. Bioinformatics 31:2035–2037. https://doi.org/10.1093/bioinformatics/btv057.
72. Bankevich A, Nurk S, Antipov D, Gurevich AA, Dvorkin M, Kulikov AS, Lesin VM, Nikolenko SI, Pham S, Prjibelski AD, Pyshkin AV, Sirotkin AV, Vyahhi N, Tesler G, Alekseyev MA, Pevzner PA. 2012. SPAdes: a new genome assembly algorithm and its applications to single-cell sequencing. J Comput Biol 19:455–477. https://doi.org/10.1089/cmb.2012.0021.
73. Li H, Durbin R. 2010. Fast and accurate long-read alignment with Burrows-Wheeler transform. Bioinformatics 26:589–595. https://doi.org/10.1093/bioinformatics/btp698.
74. Li H, Handsaker B, Wysoker A, Fennell T, Ruan J, Homer N, Marth G, Abecasis G, Durbin R, 1000 Genome Project Data Processing Subgroup. 2009. The Sequence Alignment/Map format and SAMtools. Bioinformatics 25:2078–2079. https://doi.org/10.1093/bioinformatics/btp352.
75. Murphy RR, O'Connell J, Cox AJ, Schulz-Trieglaff O. 2015. NxRepair: error correction in de novo sequence assembly using Nextera mate pairs. PeerJ 3:e996. https://doi.org/10.7717/peerj.996.
76. O'Leary NA, Wright MW, Brister JR, Ciufo S, Haddad D, McVeigh R, Rajput B, Robbertse B, Smith-White B, Ako-Adjei D, Astashyn A, Badretdin A, Bao Y, Blinkova O, Brover V, Chetvernin V, Choi J, Cox E, Ermolaeva O, Farrell CM, Goldfarb T, Gupta T, Haft D, Hatcher E, Hlavina W, Joardar VS, Kodali VK, Li W, Maglott D, Masterson P, McGarvey KM, Murphy MR, O'Neill K, Pujar S, Rangwala SH, Rausch D, Riddick LD, Schoch C, Shkeda A, Storz SS, Sun H, Thibaud-Nissen F, Tolstoy I, Tully RE, Vatsan AR, Wallin C, Webb D, Wu W, Landrum MJ, Kimchi A, et al. 2016. Reference sequence (RefSeq) database at NCBI: current status, taxonomic expansion, and functional annotation. Nucleic Acids Res 44:D733–D745. https://doi.org/10.1093/nar/gkv1189.
77. Parks DH, Chuvochina M, Rinke C, Mussig AJ, Chaumeil P-A, Hugenholtz P. 2022. GTDB: an ongoing census of bacterial and archaeal diversity through a phylogenetically consistent, rank normalized and complete genome-based taxonomy. Nucleic Acids Res 50:D785–D794. https://doi.org/10.1093/nar/gkab776.
78. Gurevich A, Saveliev V, Vyahhi N, Tesler G. 2013. QUAST: quality assessment tool for genome assemblies. Bioinformatics 29:1072–1075. https://doi.org/10.1093/bioinformatics/btt086.
79. Katoh K, Kuma K, Toh H, Miyata T. 2005. MAFFT version 5: improvement in accuracy of multiple sequence alignment. Nucleic Acids Res 33:511–518. https://doi.org/10.1093/nar/gki198.
80. Capella-Gutiérrez S, Silla-Martínez JM, Gabaldón T. 2009. trimAl: a tool for automated alignment trimming in large-scale phylogenetic analyses. Bioinformatics 25:1972–1973. https://doi.org/10.1093/bioinformatics/btp348.
81. Nguyen L-T, Schmidt HA, von Haeseler A, Minh BQ. 2015. IQ-TREE: a fast and effective stochastic algorithm for estimating maximum-likelihood phylogenies. Mol Biol Evol 32:268–274. https://doi.org/10.1093/molbev/msu300.
82. Ivica L, Peer B. 2019. Interactive Tree Of Life (iTOL) v4: recent updates and new developments. Nucleic Acids Res 47:W256–W259. https://doi.org/10.1093/nar/gkz239.
83. Edgar RC. 2004. MUSCLE: multiple sequence alignment with high accuracy and high throughput. Nucleic Acids Res 32:1792–1797. https://doi.org/10.1093/nar/gkh340.
84. Sudhir K, Glen S, Michael L, Christina K, Koichiro T. 2018. MEGA X: Molecular Evolutionary Genetics Analysis across Computing Platforms. Mol Biol Evol 35:1547–1549. https://doi.org/10.1093/molbev/msy096.
85. Hille R. 1996. The mononuclear molybdenum enzymes. Chem Rev 96:2757–2816. https://doi.org/10.1021/cr950061t.
86. Meyer O, Schlegel HG. 1978. Reisolation of the carbon monoxide utilizing hydrogen bacterium *Pseudomonas carboxydovorans* (Kistner) comb. nov. Arch Microbiol 118:35–43. https://doi.org/10.1007/BF00406071.
87. Park SW, Hwang EH, Park H, Kim JA, Heo J, Lee KH, Song T, Kim E, Ro YT, Kim SW, Kim YM. 2003. Growth of *Mycobacteria* on carbon monoxide and methanol. J Bacteriol 185:142–147. https://doi.org/10.1128/JB.185.1.142-147.2003.
88. Buchfink B, Xie C, Huson DH. 2015. Fast and sensitive protein alignment using DIAMOND. Nat Methods 12:59–60. https://doi.org/10.1038/nmeth.3176.
89. Delcher AL, Kasif S, Fleischmann RD, Peterson J, White O, Salzberg SL. 1999. Alignment of whole genomes. Nucleic Acids Res 27:2369–2376. https://doi.org/10.1093/nar/27.11.2369.
90. Aziz RK, Bartels D, Best AA, DeJongh M, Disz T, Edwards RA, Formsma K, Gerdes S, Glass EM, Kubal M, Meyer F, Olsen GJ, Olson R, Osterman AL, Overbeek RA, McNeil LK, Paarmann D, Paczian T, Parrello B, Pusch GD, Reich C, Stevens R, Vassieva O, Vonstein V, Wilke A, Zagnitko O. 2008. The RAST Server: Rapid Annotations using Subsystems Technology. BMC Genom 9:75. https://doi.org/10.1186/1471-2164-9-75.
91. Sullivan MJ, Petty NK, Beatson SA. 2011. Easyfig: a genome comparison visualizer. Bioinformatics 27:1009–1010. https://doi.org/10.1093/bioinformatics/btr039.
92. Bland C, Ramsey TL, Sabree F, Lowe M, Brown K, Kyrpides NC, Hugenholtz P. 2007. CRISPR Recognition Tool (CRT): a tool for automatic detection of clustered regularly interspaced palindromic repeats. BMC Bioinformatics 8:209. https://doi.org/10.1186/1471-2105-8-209.
93. Chan PP, Lin BY, Mak AJ, Lowe TM. 2021. tRNAscan-SE 2.0: improved detection and functional classification of transfer RNA genes. Nucleic Acids Res 49:9077–9096. https://doi.org/10.1093/nar/gkab688.
94. Lagesen K, Hallin P, Rødland EA, Staerfeldt H-H, Rognes T, Ussery DW. 2007. RNAmmer: consistent and rapid annotation of ribosomal RNA genes. Nucleic Acids Res 35:3100–3108. https://doi.org/10.1093/nar/gkm160.
95. Cripps RE, Eley K, Leak DJ, Rudd B, Taylor M, Todd M, Boakes S, Martin S, Atkinson T. 2009. Metabolic engineering of *Geobacillus thermoglucosidasius* for high yield ethanol production. Metab Eng 11:398–408. https://doi.org/10.1016/j.ymben.2009.08.005.